We are IntechOpen,
the world's leading publisher of
Open Access books
Built by scientists, for scientists

4,800
Open access books available

122,000
International authors and editors

135M
Downloads

Our authors are among the

154
Countries delivered to

TOP 1%
most cited scientists

12.2%
Contributors from top 500 universities

Interested in publishing with us?
Contact book.department@intechopen.com

Numbers displayed above are based on latest data collected.
For more information visit www.intechopen.com

Laser Probe 3D Cameras Based on Digital Optical Phase Conjugation

Zhiyang Li
College of Physical Science and Technology, Central China Normal University
Hubei, Wuhan,
P. R. China

1. Introduction

A camera makes a picture by projecting objects onto the image plane of an optical lens, where the image is recorded with a film or a CCD or CMOS image sensor. The pictures thus generated are two-dimensional and the depth information is lost. However in many fields depth information is getting more and more important. In industry the shape of a component or a die, needs to be measured accurately for quality control, automated manufacturing, solid modelling, etc. In auto-navigation, three dimensional coordinates of changing environment need to be acquired in real-time to aid auto path planning for vehicles or intelligent robots. In driving assistant systems any obstacle in front a car should be detected within 0.01 second. Even in making 3D movies for true 3D display in the near future, three dimensional coordinates need to be recorded with a fame rate of at least 25f/s, etc. For the past few decades intensive researches have been carried out and various optical methods have been investigated[Chen, et al., 2000], yet they still could not fulfil every requirement of present-day applications on either measuring speed, or accuracy, or measuring range/area, or convenience, etc. For example, although interferometric methods provide very high measuring precision [Yamaguchi, et al., 2006; Barbosa, & Lino, 2007], they are sensitive to speckle noise and vibration and perform measurement over small areas. The structured light projection methods provide good precision and full field measurements [Srinivasan, et al., 1984; Guan, et al., 2003], yet the measuring width is still limited to several meters. Besides they often encounter shading problems. Stereovision is a convenient means for large field measurements without active illumination, but stereo matching often turns very complicated and results in high reconstruction noise [Asim, 2008].To overcome the drawbacks improvements and new methods appear constantly. For example, time-of-flight (TOF) used to be a point-to-point method [Moring, 1989]. Nowadays commercial 3D-TOF cameras are available [Stephan, et al., 2008]. Silicon retina sensors have also been developed which supports event-based stereo matching [Jürgen & Christoph, 2011]. Among all the efforts those employing cameras appear more desirable because they are non-contact, relatively cheap, easy to carry out, and provide full field measurements, etc.

The chapter introduces a new camera—a so-called laser probe 3D camera, a camera enforced with hundreds and thousands of laser probes projected onto objects, whose pre-known positions help to determine the three dimensional coordinates of objects under

investigation. The most challenging task in constructing such a 3D camera is the generation of those huge number of laser probes, with the position of each laser probe independently adaptable according to the shape of an object. In section 2 we will explain how the laser probes could be created by means of digital optical phase conjugation, an accurate method for optical wavefront reconstruction we put forward a little time earlier[Zhiyang, 2010a,2010b]. In section 3 we will demonstrate how the laser probes could be used to construct 3D cameras dedicated for various applications, such as micro 3D measurement, fast obstacle detection, 360-deg shape measurement, etc. In section 4 we will discuss more characteristics like measuring speed, energy consumption, resistance to external interferences, etc., of laser probe 3D cameras. Finally a short summery is given in section 5.

2. Generation of laser probes via digital optical phase conjugation

To build a laser-probe 3D camera, one needs first to find a way to project simultaneously hundreds and thousands of laser probes into preset positions. Looking the optical field formed by all the laser probes as a whole it might be regarded as a problem of optical wavefront reconstruction. Although various methods for optical wavefront reconstruction have been reported, few of them could fulfil above task. For example, an optical lens system can focus a light beam and move it around with a mechanical gear. But it can hardly adjust its focal length so quickly to produce so many laser probes far and near within the time of a snapshot of a camera. Traditional optical phase conjugate reflection is an efficient way for optical wavefront reconstruction [Yariv, & Peper, 1977; Feinberg, 1982]. However it reproduces, or reflects only existing optical wavefronts based on some nonlinear optical effects. That is to say, to generate above mentioned laser probes one should first find another way to create beforehand the same laser probes with high energy to trig nonlinear optical effect. While holography can reconstruct only static optical wavefronts since high resolution holographic plates have to be used.

To perform real-time digital optical wavefront reconstruction it is promising to employ spatial light modulators (SLM) [Amako, et al. 1993; Matoba, et al. 2002; Kohler, et al. 2006]. A SLM could modulate the amplitude or phase of an optical field pixel by pixel in space. For liquid crystal SLMs several millions of pixels are available. And the width of each pixel might be fabricated as small as 10 micrometers in case of a projection type liquid crystal panel. However the pixel size appears still much larger than the wavelength to be employed in a laser probe 3D camera. According to the sensitive wavelength range of a CCD or CMOS image sensor it is preferable to produce laser probes with a wavelength in the range of 0.35~1.2 micrometers, or 0.7~1.2 micrometers to avoid interference with human eyes if necessary. So the wavelength is about ten times smaller than the pixel pitch of a SLM. Therefore with bare SLMs only slowly varying optical fields could be reconstructed with acceptable precision. Unfortunately the resulting optical field formed by hundreds and thousands of laser probes may appear extremely complex.

Recently we introduced an adiabatic waveguide taper to decompose an optical field, however dramatically it changes over space, into simpler form that is easier to rebuild [Zhiyang, 2010a]. As illustrated in Fig.1, such an adiabatic taper consists of a plurality of single-mode waveguides. At the narrow end of the taper the single-mode waveguides couple to each other. While at the wide end the single-mode waveguides become optically isolated from each other. When an optical field incidents on the left narrow end of the taper,

it would travel to the right wide end and gets decomposed into fundamental mode field of each isolated single-mode waveguide. Since these fundamental mode fields are separated from each other in space, they could be reconstructed using a pair of low resolution SLMs and a micro lens array (MLA) as illustrated in Fig.2.
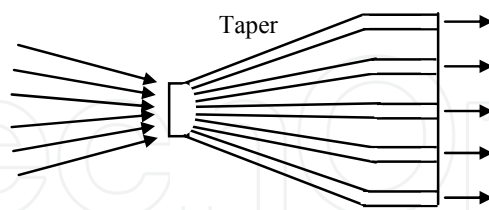

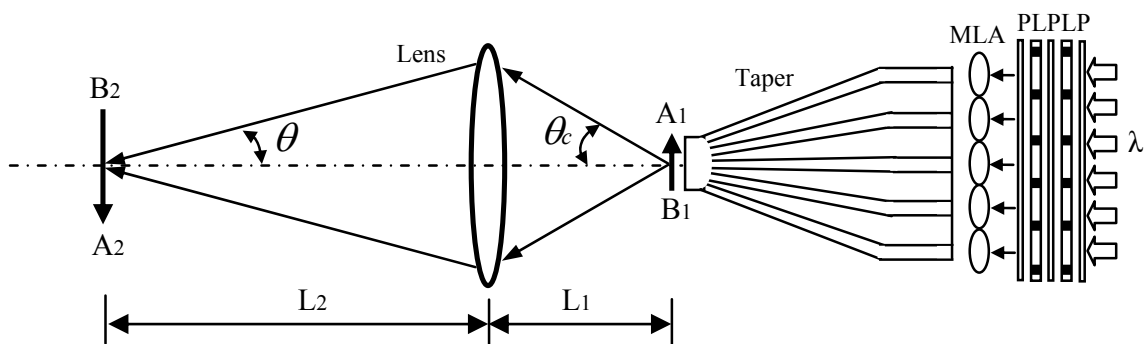Fig. 1. Structure of an adiabatic waveguide taper.

Fig. 2. Device to perform digital optical phase conjugation.

For the device in Fig.2 we may adjust the gray scale of each pixel of SLMs so that it modulates the amplitude and the phase of illuminating laser beam properly [Neto, et al. 1996; Tudela, et al. 2004] and reconstruct a conjugate field proportional to above decomposed fundamental mode field within each isolated single-mode waveguide at the right wide end. Due to reciprocity of an optical path the digitally reconstructed conjugate light field within each isolated single-mode waveguide would travel inversely to the left narrow end of the taper, combine and create an optical field proportional to the original incident optical field. Since the device in Fig.2 rebuilds optical fields via digital optical phase conjugation, it gets ride off all the aberrations inherent in conventional optical lens systems automatically. For example, suppose an object A_2B_2 is placed in front of the optical lens. It forms an image A_1B_1 with poor quality. The reconstructed conjugate image in front of the narrow end of the taper bears all the aberrations of A_1B_1. However, due to reciprocity, the light exited from the reconstructed conjugate image of A_1B_1 would follow the same path and return to the original starting place, restoring A_2B_2 with exactly the same shape. So the resolution of a digital optical phase conjugation device is merely limited by diffraction, which can be described by,

$$dx = \frac{\lambda}{2\sin\theta} \tag{1}$$

where θ is the half cone angle of the light beam arriving at a point at image plane as indicated in Fig.2. The half cone angle θ could be estimated from the critical angle θ_c of

incidence of the taper through the relation $\tan(\theta)/\tan(\theta_c)=L_1/L_2=|A_1B_1|/|A_2B_2| = 1/\beta_x$, where β_x being the vertical amplification ratio of the whole optical lens system. When SLMs with 1920x1080 pixels are employed, the width of the narrow end of an adiabatic waveguide taper with a refraction index of 1.5 reaches 0.458mm for $\lambda=0.532$ µm, or 0.860mm for $\lambda=1$ µm respectively to support Ns=1920 guided eigenmodes. When a 3x3 array of SLMs with same pixels are employed, the width of the narrow end of the taper increases to 1.376mm for $\lambda=0.532$ µm, or 2.588mm for $\lambda=1$ µm respectively to support a total of Ns=3x1920=5760 guided eigenmodes. The height of reconstructed conjugate image A_1B_1 right in front of the narrow end of the tap may have the same size as the taper. Fig.3 plotted the lateral resolutions at different distances Z from the taper (left), or for different sizes of reconstructed image A_2B_2(middle and right) with θ_c =80°, where the resolution for $\lambda=0.532$ µm is plotted in green colour and that for $\lambda=1$ µm in red colour. It could be seen that within a distance of Z=0~1000 µm, the resolution is jointly determined by wavelength and the pixel number Ns of the SLMs. The optical lens is taken away temporarily since there is no room for it when Z is less than 1mm. However when $|A_2B_2|$ is larger than 40mm, the resolution becomes irrelevant to wavelength, but decreases linearly with the pixel number Ns of the SLMs and increase linearly with the size of $|A_2B_2|$. When $|A_2B_2|$=100m, the resolution is about 10.25mm for Ns=1920 and 3.41mm for Ns=5760 respectively.

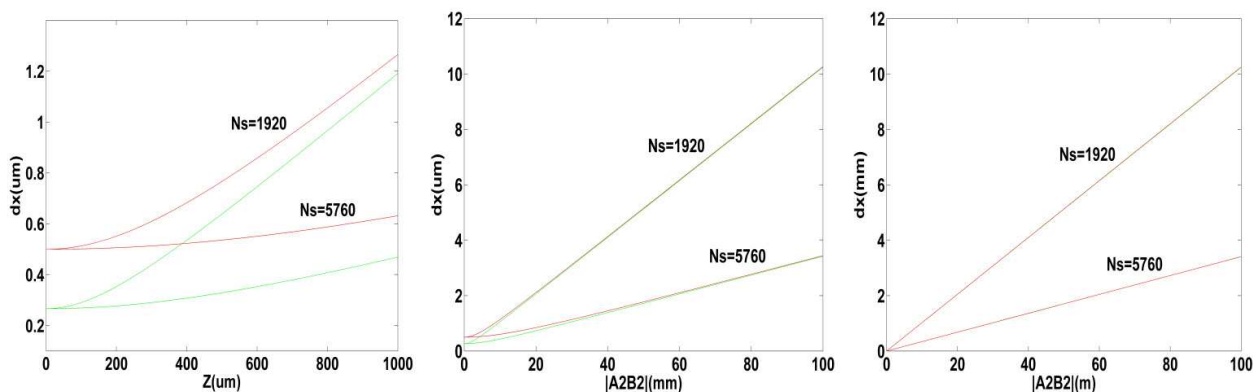Fig. 3. Lateral resolution of a laser probe at a distance Z in the range of 0~1000µm (left); or with $|A_2B_2|$ in the range of 1~100mm(middle); and 0.1~100m(right) for $\lambda=0.532$ µm(green line) and $\lambda=1$ µm (red line).

To see more clearly how the device works, Fig.4 simulated the reconstruction of a single light spot via digital optical phase conjugation. The simulation used the same software and followed the same procedure as described in Ref.[Zhiyang, 2010a]. In the calculation $\lambda=1.032$µm, the number of eigenmodes equals 200 and the perfectly matched layer has a thickness of - 0.15i. The adiabatic waveguide taper has a refraction index of 1.5. To save time only the first stack of the taper, which has a height of 20 micrometers and a length of 5 micrometers, was taken into consideration. A small point light source was placed 25 micrometers away from the taper in the air. As could be seen from Fig.4a, the light emitted from the point light source propagates from left to right, enters the first stack of the taper and stimulates various eigenmodes within the taper. The amplitudes and phases of all the guided eigenmodes on the right side end of the first stack of the taper were transferred to their conjugate forms and used as input on the right side. As could be seen from Fig.4b the light returned to the left side and rebuilt a point light source with expanded size.
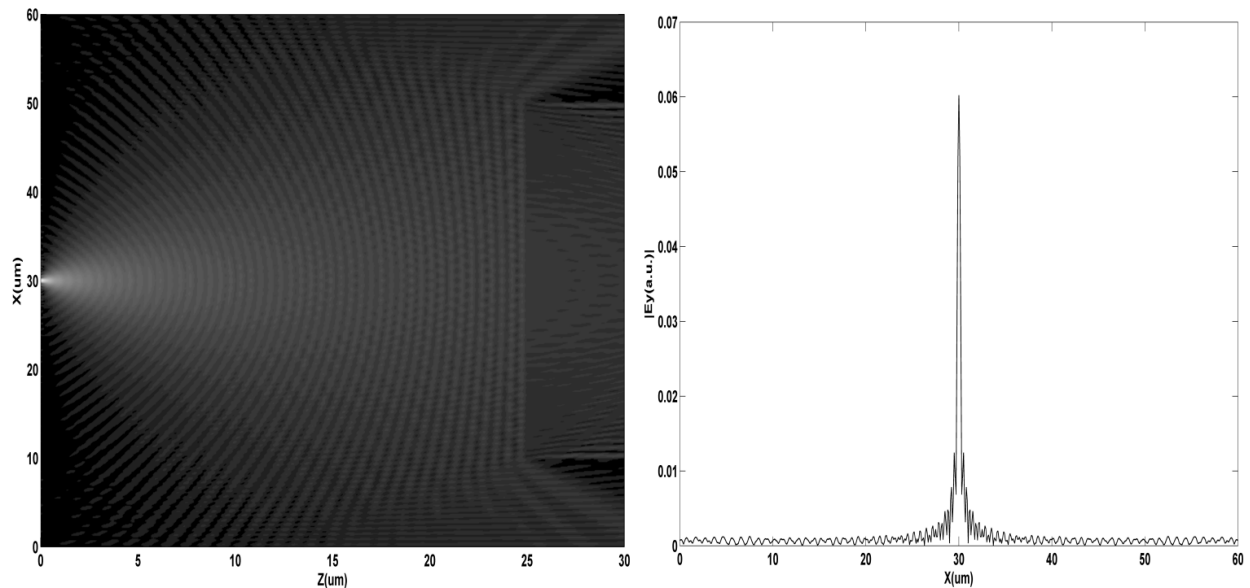
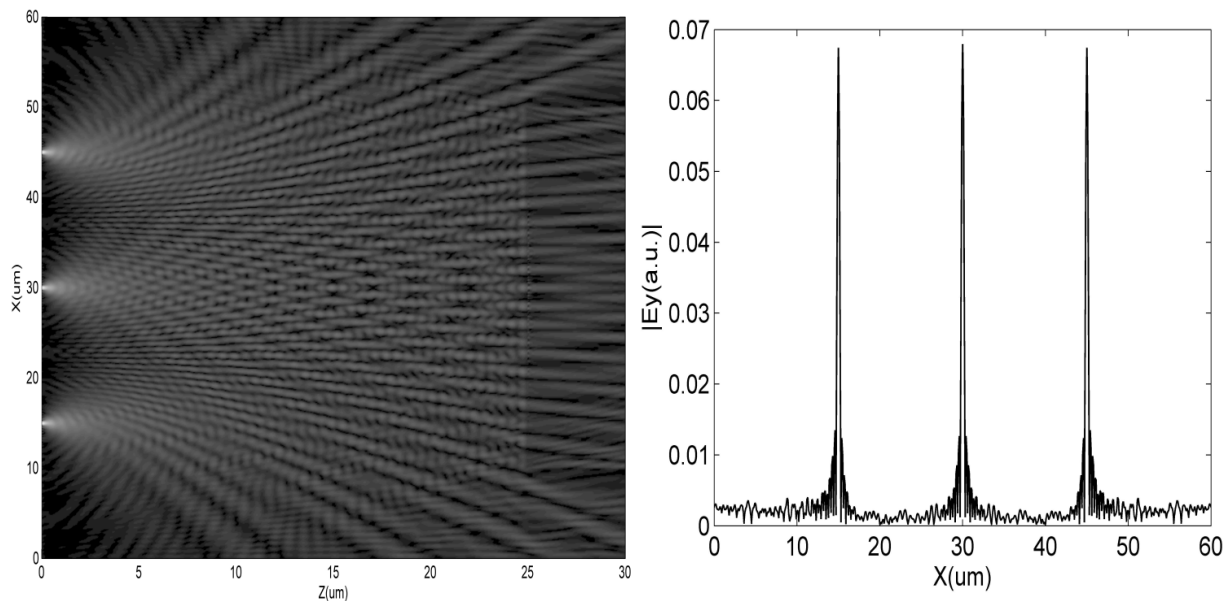(a). Distribution for incident light, left: 2-D field; right:1-D Electrical component at Z=0
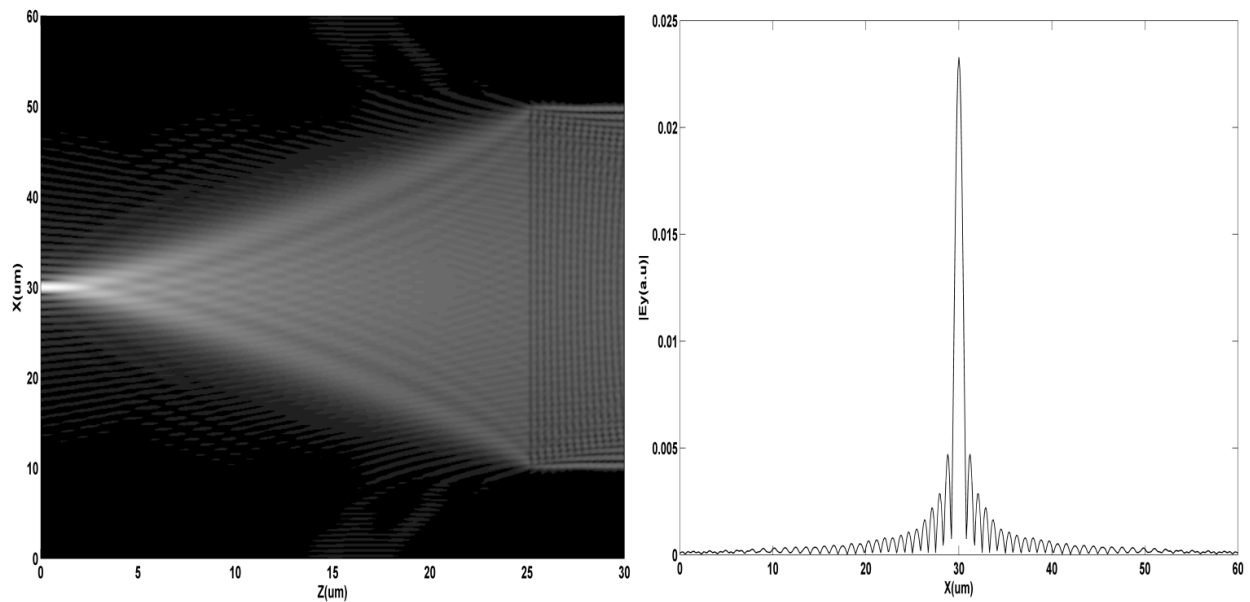
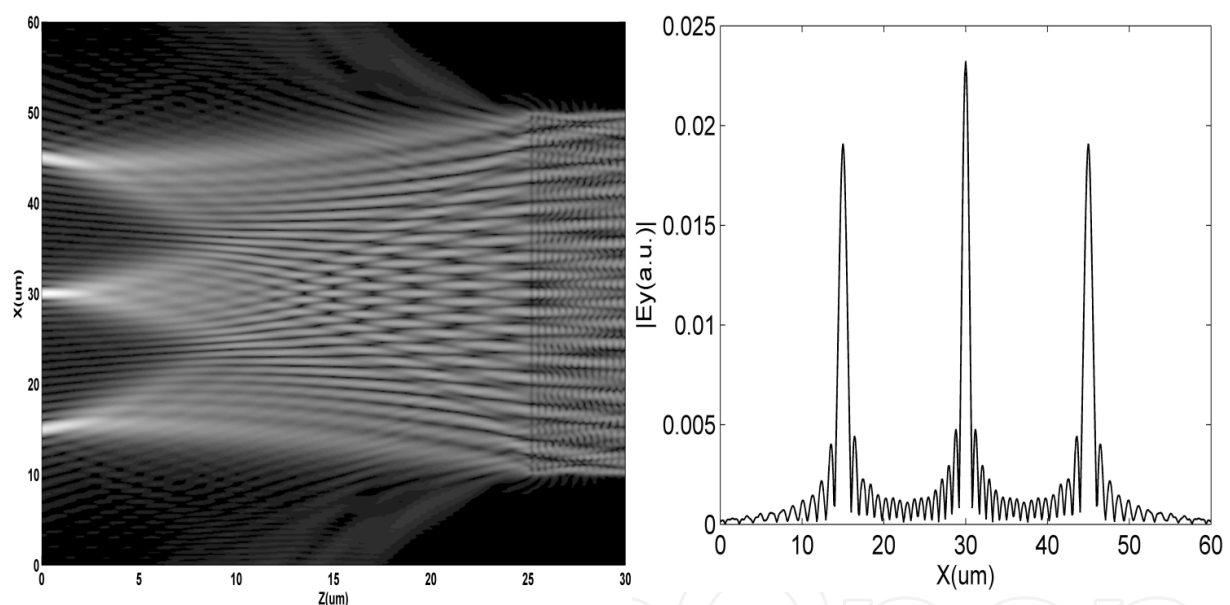(b). Distribution for rebuilt light, left: 2-D field; right:1-D Electrical component at Z=0

Fig. 4. Reconstruction of a single light spot via digital optical phase conjugation.

From the X-directional field distribution one can see that the rebuilt light spot has a half-maximum-width of about 1μm, which is very close to the predicated resolution of 0.83μm by Eq.1, if the initial width of the point light source is discounted.

Fig.5 demonstrated how multiple light spots could be reconstructed simultaneously via digital optical phase conjugation. The simulation parameters were the same as in Fig.4. Three small point light sources were placed 25 micrometers away from the taper and separated 15 micrometers from each other along vertical direction. As could be seen from Fig.5a, the lights emitted from the three point light sources propagate from left to right, enter the first stack of the taper and stimulate various eigenmodes within the taper.

(a). Distribution for incident light, left: 2-D field; right:1-D Electrical component at Z=0

(b). Distribution for rebuilt light, left: 2-D field; right:1-D Electrical component at Z=0

Fig. 5. Reconstruction of three light spots via digital optical phase conjugation.

The amplitudes and phases of all the guided eigenmodes on the right side end of the first stack of the taper were recorded. This can also be done in a cumulative way. That is, at one time place one point light source at one place and record the amplitudes and phases of stimulated guided eigenmodes on the right side. Then for each stimulated guided eigenmode sum up the amplitudes and phases recorded in successive steps. Due to the linearity of the system the resulting amplitudes and phases for each stimulated guided eigenmode appear the same as that obtained by placing all the three point light sources at their paces at a time. Next the conjugate forms of above recorded guided eigenmodes were used as input on the right side. As could be seen from Fig.5b the light returned to the left side and rebuilt three point light sources at the same position but with expanded size. As

explained in Ref. [Zhiyang, 2010a] more than 10000 light spots could be generated simultaneously using 8-bit SLMs. Each light spot produces a light cone, or a so called laser probe.

3. Configurations of laser-probe 3D cameras

Once large number of laser probes could be produced we may employ them to construct 3D cameras for various applications. Four typical configurations, each dedicated to a particular application, have been presented in following four subsections. Subsection 3.1 provided a simple configuration for micro 3D measurement, while Subsection 3.2 focused on fast obstacle detection in a large volume for auto-navigation and safe driving. The methods and theory set up in section 3.2 also apply in rest subsections. Subsection 3.3 discussed the combination of a laser probe 3D camera with stereovision for full field real-time 3D measurements. Subsection 3.4 discussed briefly strategies for accurate static 3D measurements, including large size and 360-deg shape measurements for industry inspection. The resolution for each configuration was also analyzed.

3.1 Micro 3D measurement

To measure three dimensional coordinates of a micro object, we may put it under a digital microscope and search the surface with laser probes as illustrated in Fig.6. When the tip of a laser probe touches the surface it produces a light spot with minimum size and the preset position Z_0 of the tip stands for the vertical coordinate of the object. When the tip lays at a height of ΔZ below or above the surface, the diameter of the light spot scattered by the surface expand to Δd. From the geometric relation illustrated in Fig.6 it is easy to see that,

$$\Delta Z = \frac{Z_0}{d} \Delta d \tag{2}$$

where d is the width of the narrow end of an adiabatic waveguide taper. From Eq.2 it is clear that the depth resolution depends on the minimum detectable size of Δd. The minimum detectable size on the image plane of the objective lens is limited by the pixel size of CCD or CMOS image sensor as W_0/N_0, where W_0 is the width of an image sensor that contains N_0 pixels. When mapped back onto object plane, the minimum detectable size of Δd is $W_0/\beta N_0$,
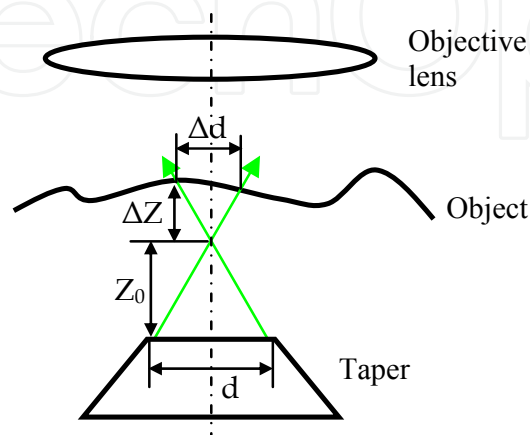

Fig. 6. Set-up for micro 3D measurement with laser probes incident from below the object.

where β is the amplification ratio of the objective lens. However if $W_0/\beta N_0$ is less than the optic aberration, which is approximately $\lambda/2NA$ for a well designed objective lens with a numerical aperture NA, the minimum detectable size of Δd is limited instead by $\lambda/2NA$.

Using Eq.2 we can estimate the resolution of ΔZ. As discussed in previous section, when SLMs with 1920×1080 pixels are employed, the width of the narrow end of an adiabatic waveguide taper with a refraction index of 1.5 reaches d=0.458mm for λ=0.532 µm. When a 3×3 array of SLMs with same pixels are employed, d increases to 1.376mm. Assuming that a 1/2 inch wide CMOS image sensor with 1920×1080 pixels is placed on the image plane of the objective lens, we have $W_0/N_0 \approx 12.7mm/1920 = 6.6µm$. For typical ×4(NA=0.1), ×10(NA=0.25), ×40(NA=0.65) and ×100(NA=1.25) objective lenses, the optic aberrations are about 2.66, 1.06, 0.41, and 0.21µm respectively. At a distance of Z_0=1mm, according to Eq.2, the depth resolutions of ΔZ for above ×4,×10,×40,×100 objective lenses are 5.81, 2.32, 0.89, and 0.46µm for d=0.458mm, or 1.93, 0.77, 0.30, and 0.15µm for d=1.376mm respectively.

In above discussion we have not taken into consideration the influence of the refraction index of the transparent object. Although it is possible to make a proper compensation for the influence once the refraction index is known, there is another way to avoid it by inserting the narrow end of an adiabatic waveguide taper above the objective lens. This could be done with the help of a small half–transparent-half-reflective beam splitter M as illustrated in Fig.7. It is of better depth resolution due to increased cone angle of laser probes at the cost of trouble some calibration for each objective lens. When searching for the surface of an object, the tips of laser probes push down slowly toward object. From monitored successive digital images it is easy to tell when a particular laser probe touches a particular place on the object. Since the laser probes propagate in the air, the influence of the internal refraction index of the object is eliminated.
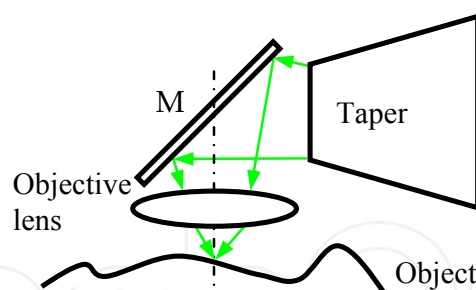

Fig. 7. Set-up for micro 3D measurement with laser probes incident from above the objective lens.

By the way, besides discrete laser probes, a laser probe generating unit could also project structured light beams. That means a laser probe 3D camera could also work in structured light projection mode. It has been demonstrated that by means of structured light projection a lateral resolution of 1µm and a height resolution of 0.1µm could be achieved [Leonhardt, et at. 1994].

3.2 Real-time large volume 3D detection

When investigating a large field, we need to project laser probes into far away distance. As a result the cone angles of the laser probes would become extremely small. A laser probe

might look like a strait laser stick, which makes it difficult to tell where the tip is. In such a case we may use two laser probe generating units and let the laser probes coming from different units meet at preset positions. Since the two laser probe generating units could be separated with a relatively large distance, the angle between two laser probes pointing to the same preset position may increase greatly. Therefore the coordinates of objects could be determined with much better accuracy even if they are located at far distances.

Fig.8 illustrated the basic configuration of a laser probe 3D camera constructed with two laser probe generating units $U_{1,2}$ and a conventional CMOS digital camera C. The camera C lies in the middle of $U_{1,2}$. In Fig.8 the laser probe generating unit U_1 emits a single laser probe as plotted in red line while U_2 emits a single laser probe as plotted in green line. The two laser probes meet at preset point A. An auxiliary blue dashed ray is drawn, which originates at the optic centre of the optical lens of the camera C and passes though point A. It is understandable that all the object points lying along the blue dashed line will come onto the same pixel A' of the CMOS image sensor. If an object lies on a plane P_1 in front of point A, the camera captures two light spots, with the light spot produced by red laser probe lying at a pixel distance of -Δj_1 on the right side of A' and the light spot produced by green laser probe lying at a pixel distance of -Δj_2 on the left side of A' as illustrated in Fig.9a. When an object lies on a plane P_2 behind point A, the light spots produced by the red and green laser probes exchange their position as illustrated in Fig.9c. When an object sits right at point A the camera captures a single light spot at A' as illustrated in Fig.9b. Suppose the digital camera C in Fig.8 has a total of N pixels along horizontal direction, which cover a scene with a width of W at distance Z, the X-directional distance Δd_1 (or Δd_2) between a red (or green) laser probe and a blue dashed line in real space could be estimated from the pixel distance Δj_1 (or Δj_2) on the captured image by,

$$\Delta d_{1,2} = \frac{W}{N}\Delta j_{1,2} = \frac{2Ztg\alpha}{N}\Delta j_{1,2} \tag{3}$$

where α is the half view angle. As illustrated in Fig.8 and Fig.9a-c, $\Delta d_{1,2}$ is positive when the light spot caused by red (or green) laser probe laying at the left (or right) side of A'. For illustrative purpose the laser probes emitted from different units are plotted in different
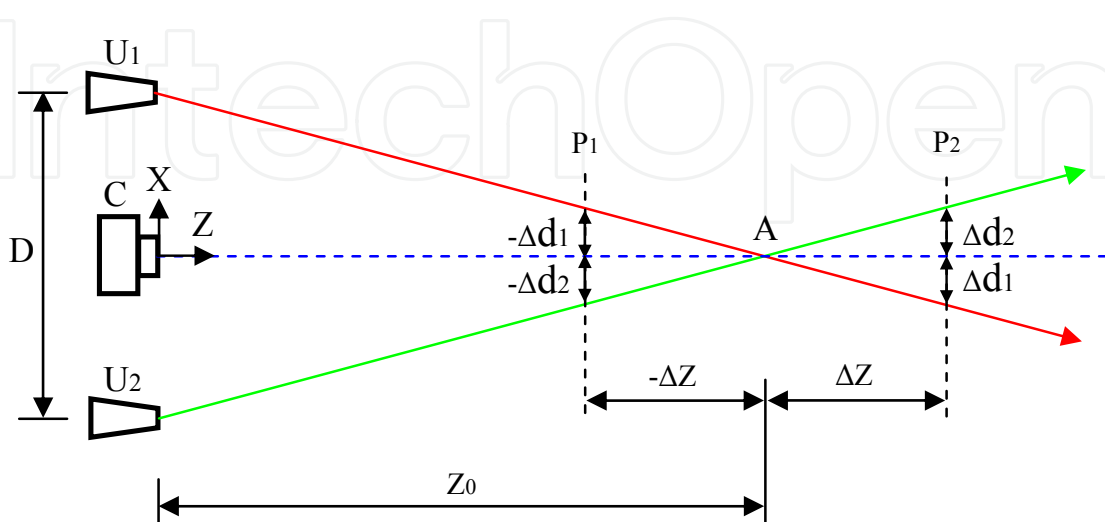

Fig. 8. Basic configuration of a laser probe 3D camera.

colours. In a real laser probe 3D camera all the laser probes may have the same wavelength. To distinguish them we may set the laser probes emitted from one unit slightly higher in vertical direction than the laser probes emitted from another unit as illustrated in Fig.9d-f.
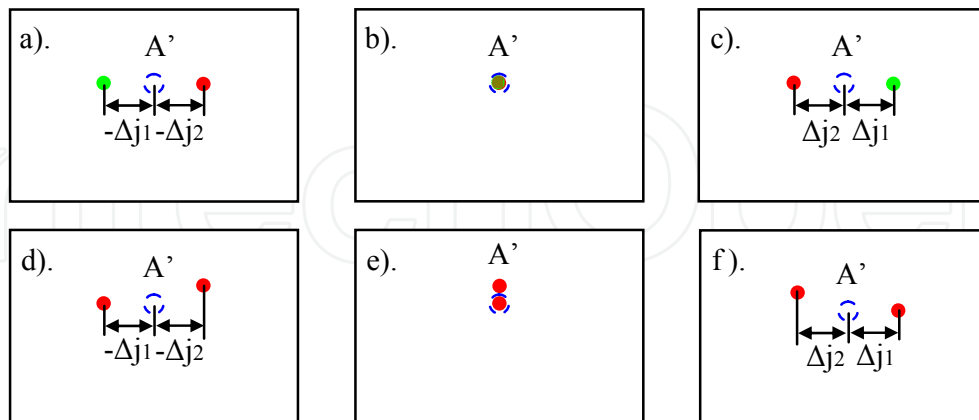

Fig. 9. Images of laser probes reflected by an object located at different distances. Left: in front of A; Middle: right at A; Right: behind A.

From X-directional distance $\Delta d_{1,2}$ it is easy to derive the Z-directional distance ΔZ of the object from the preset position A using the geometric relation,

$$\frac{\Delta d_{1,2}}{\Delta Z} = \frac{D}{2Z_0} \tag{4}$$

where D is the space between two laser probe generating units $U_{1,2}$, Z_0 being the preset distance of point A. From Eq.3-4 it is not difficult to find,

$$Z = Z_0 + \Delta Z = \frac{DNZ_0}{DN - 4Z_0 tg\alpha \Delta j_{1,2}} \tag{5}$$

After differentiation and some rearrangement, Eq.5 yields,

$$dZ = \frac{4Z^2 tg\alpha}{DN} dj_{1,2} \tag{6}$$

where dZ and $dj_{1,2}$ are small deviations, or measuring precisions of ΔZ and $\Delta j_{1,2}$ respectively. In Eq.6 it is noticeable that the preset distance Z_0 of a laser probe exerts little influence on the measuring precisions of ΔZ. Usually $\Delta j_{1,2}$ could be measured with half pixel precision. Assuming D=1000mm, $tg\alpha$=0.5 and $dj_{1,2}$=0.5, Fig.10 plotted the calculated precision dZ based on Eq.6 when a commercial video camera with 1920×1080 pixels, N= 1920 (in blue line), or a dedicated camera with 10k×10k pixels, N= 10k(in red line) is employed. As could be seen from Fig.10 the depth resolution changes with the square of object distance Z. At a distance of 100,10, 5, and 1m, the depth resolutions are 5263, 53, 13, and 0.5mm for N=1920, which reduce to 1000, 10, 2.5, and 0.1mm respectively for N=10k. The depth resolutions are acceptable in many applications considering the field is as wide as 100 m at a distance of 100 mm. From Eq.6 it is clear that to improve the depth resolution one can increase D or N, or both. But the most convenient way is to decrease α, that is, to make a close-up of the object. For example, when $tg\alpha$ decreases from 0.5 to 0.05, the measuring precision of Z would

improve by 10 times. That is to say, a 0.5m wide object lying at a distance of 5m from the camera could be measured with a depth precision of 1.3mm (N= 1920), or 0.25mm(N=10k), if its image covers the whole area of the CCD or CMOS image sensor.
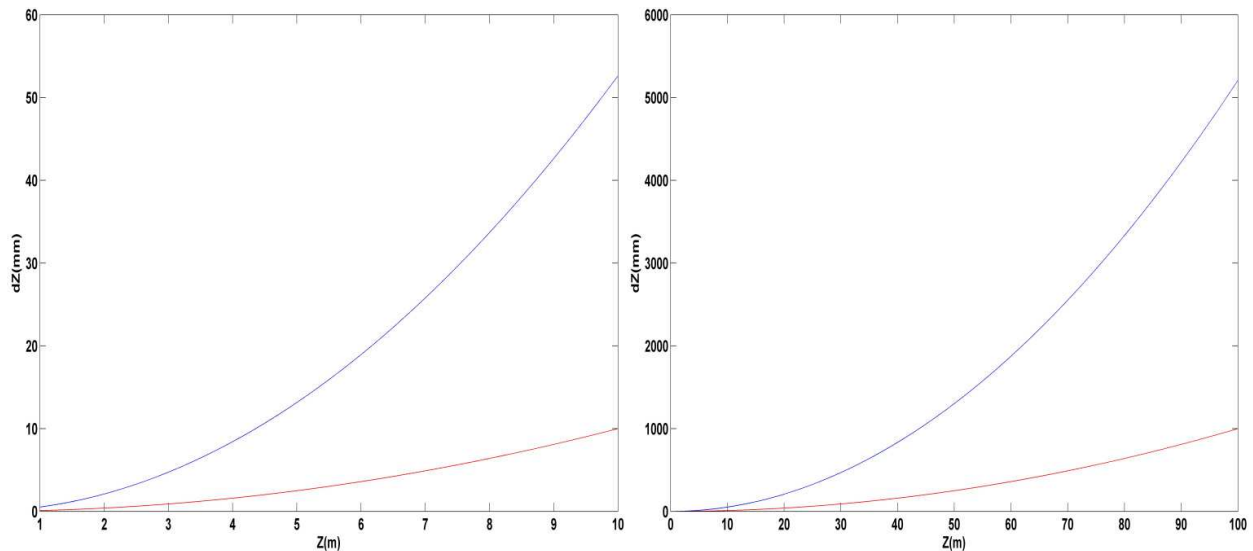

Fig. 10. Depth resolution of a laser probe 3D camera in the range of 0~10m(left) and 0~100m(right) with D=1000mm, $tg\alpha$=0.5, dj$_{1,2}$=0.5, and N=1920(blue) or 10k(red).

To acquire the three dimensional coordinates of a large scene the laser probe generating units should emit hundreds and thousands of laser probes. For convenience, in Fig.8 only one laser probe is shown for each unit. In Fig.11 six laser probes are plotted for each unit. It
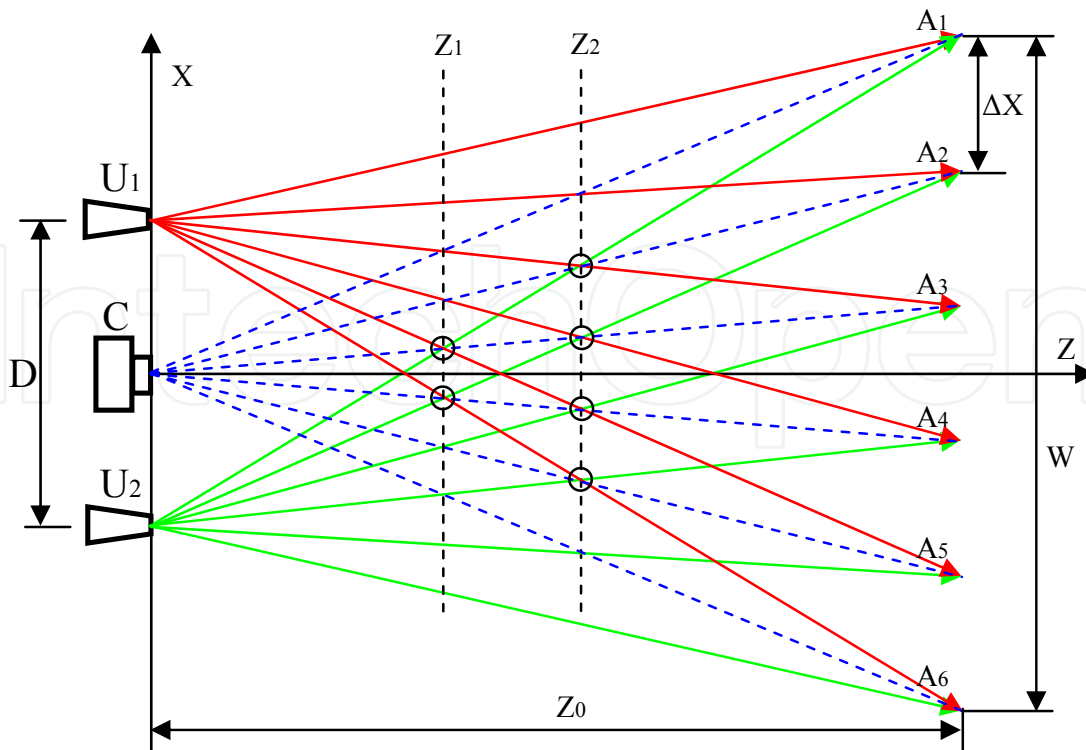

Fig. 11. Propagations of laser probes with preset destinations at distance Z_0.

is easy to see that as the number of laser probes increases the situation becomes quite complicated. It is true that each laser probe from one unit meets with one particular laser probe from another unit at six preset points A_{1-6} respectively. However the same laser probe would also come across other five laser probes from another unit at points other than A_{1-6}. Actually, if each laser probe generating unit produces N_p laser probes, a total of $N_p \times N_p$ cross points will be made by them, and only N_p points among them are at preset positions. The other $(N_p - 1) \times N_p$ undesired cross points might probably cause false measurements. See the two cross points on plane Z_1 and four cross points on plane Z_2 that are marked with small black circles, we could not distinguish them from preset points A_{2-5}, since they all sit on the blue dashed lines, sharing the same preset pixel positions on captured images. As a result it will be impossible to tell whether the object is located around the preset points A_{1-6} or near the plane Z_1 or Z_2. To avoid this ambiguity we should first find where the plane Z_1 or Z_2 is located.

As illustrated in Fig.11, since the optic centre of the optical lens of digital camera C is placed at the original point (0,0), the X-Z coordinates of the optic centres of the two laser probe emitting units $U_{1,2}$ becomes (D/2,0) and (-D/2,0) respectively. Denoting the X-Z coordinates of N_p preset points A_i as (X_i, Z_0), $i=1,2,\ldots,N_p$, the equations for red, blue and green lines could be written respectively as,

$$X = \frac{D}{2} + (X_i - \frac{D}{2})\frac{Z}{Z_0} \qquad i = 1,2,\ldots,N_P \qquad (7)$$

$$X = X_j\frac{Z}{Z_0} \qquad j = 1,2,\ldots,N_P \qquad (8)$$

$$X = -\frac{D}{2} + (X_k + \frac{D}{2})\frac{Z}{Z_0} \qquad k = 1,2,\ldots,N_P \qquad (9)$$

where i, j and k are independent indexes for preset points A_i, A_j and A_k. The cross points where a red line, a blue line and a green line meet could be find by solving the linear equations Eq.7-9, which yields,

$$Z = \frac{D}{D + X_k - X_i}Z_0 \qquad (10a)$$

$$X = X_j\frac{Z}{Z_0} \qquad (10b)$$

$$X_j = \frac{X_k + X_i}{2} \qquad (10c)$$

When $X=X_i=X_j=X_k$, according to Eq.10a, $Z=Z_0$. They stand for the coordinates of N_p preset points. When $X_k \neq X_i$, we have $Z \neq Z_0$, which gives the coordinates of cross points that cause ambiguity, like the cross points marked with black circles on plane Z_1 or Z_2 in Fig.11.

One way to eliminate above false measurements is to arrange more laser probes with preset destinations at different Z_0 that helps to verify whether the object is located near the preset

points. To avoid further confusion it is important that laser probes for different Z_0 should be arranged on different planes as indicated in Fig.12. For laser probes arranged on the same plane perpendicular to Y-Z plane they share the same cut line on Y-Z plane. Since the optic centres of the two laser probe emitting units $U_{1,2}$ and the optical lens of digital camera C all sit at (0, 0) on Y-Z plane, if we arrange the laser probes for a particular distance Z_0 on the same plane perpendicular to Y-Z plane, they will come across with each other on that plane with no chance to come across with other laser probes arranged on other planes perpendicular to Y-Z plane.
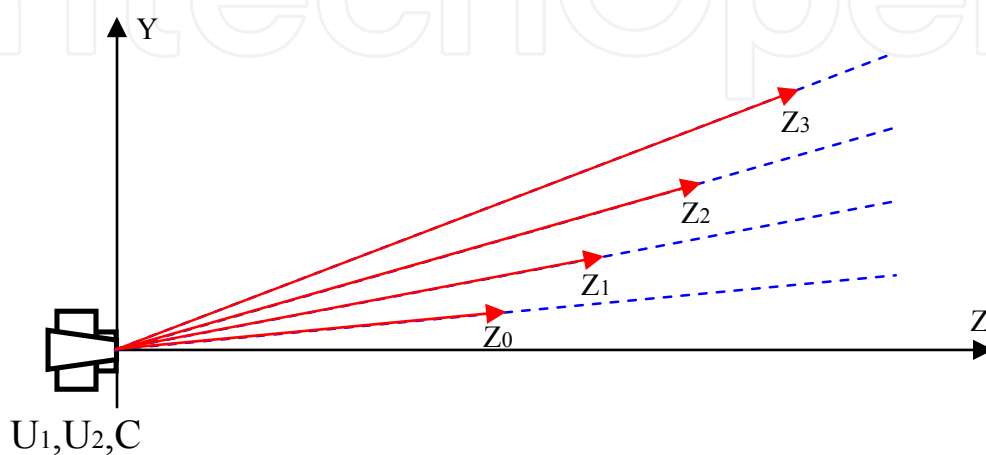

Fig. 12. Laser probes arranged on different planes perpendicular to Y-Z plane.

In what follows, we will design a laser probe 3D camera for auto-navigation and driving assistant systems, demonstrating in detail how the laser probes could be arranged to provide accurate and definite depth measurement. In view of safety a 3D camera for auto-navigation or driving assistant systems should detector obstacles in very short time and acquiring three dimensional coordinates within a range from 1 to 100m and a relatively large view angle 2α. In following design we let $\alpha \approx 26.6^\circ$, so that $tg\alpha=0.5$. Since the device is to be mounted within a car, we may chose a large separation for two laser probe generating units as D=1m, which provides a depth resolution as plotted in Fig.10. To avoid above false measurements we project laser probes with preset destinations at seven different planes at Z_0=2,4,8,14,26,50, and 100m. In addition the X-directional spaces between adjacent preset destinations are all set as $\Delta X=X_i-X_{i+1}$=2m, where the preset destination with lower index number assumes larger X coordinate. The propagations of these laser probes in the air are illustrated in Fig.13-14. In Fig.13 the propagations of the laser probes over a short range between zero to the preset destinations are drawn on the left side, while the propagations of the same laser probes over the entire range between 0~100m are drawn on the right side. In Fig.14 only the propagations of the laser probes over the entire range between 0~100m are shown. The optic centres of the first and second laser probe generating units $U_{1,2}$ are located at (0.5,1) and (-0.5,0) respectively, while the camera C sits at the original point (0,0). The red and green lines stand for the laser probes emitted from U_1 and U_2 respectively. The solid blue lines connect the optic centre of the optical lens with the preset destinations of the laser probes on a given plane at Z_0, which plays the same auxiliary function as the dashed blue lines in Fig.8.
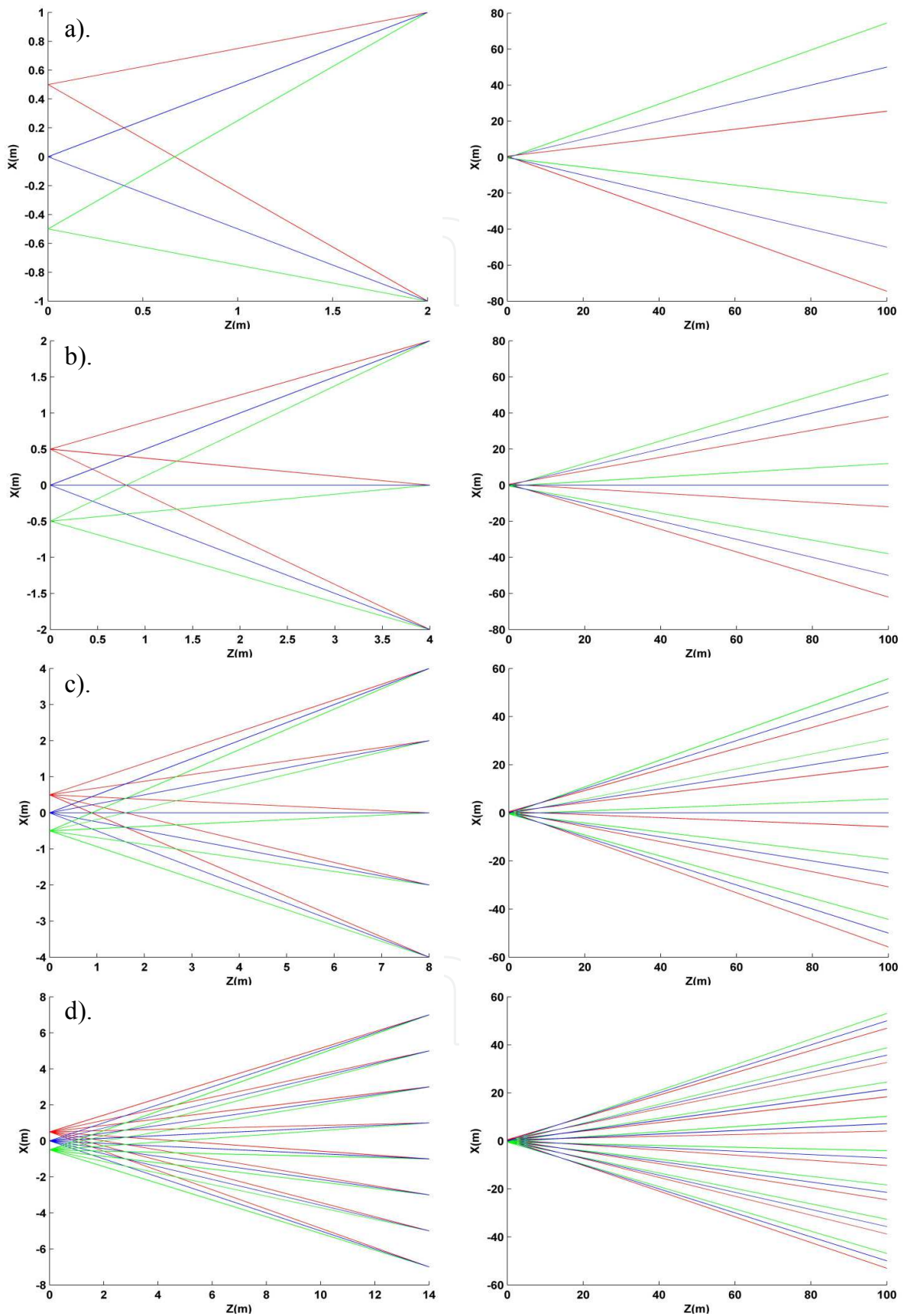
Fig. 13. Propagations of laser probes with destinations at a). 2m; b). 4m; c). 8m; and d). 14m.

First lets check Fig.13a for Z_0=2m. Since $\Delta X=X_i-X_{i+1}$=2m, Eq.10a becomes,

$$Z = \frac{1}{1 + (k-i)\Delta X} Z_0 = \frac{1}{1+2n} Z_0 \qquad (11)$$

where n=k-i is an even integer. For an odd integer of n Eq.10c does not hold true. Therefore $Z \leq Z_0/5$, if n≠0, which implies that all the possible undesired cross points are located much closer to the camera C. In addition since the field width at Z_0 is $W=2Z_0 tg\alpha = Z_0$, the total number of laser probes that could be arranged within a width of W is

$$N_P = \frac{W}{\Delta X} + 1 = \frac{Z_0}{2} + 1 \qquad (12)$$

According to Eq.12, N_P=2 at Z_0=2m. As the maximum value for n in Eq.11 is $N_P-1=1$ and n should be even integer, we have n=0. It means that beside 2 preset points there are no other cross points. In Fig.13a, from the left figure we see only two cross points at preset destinations at 2m. We find no extra cross points in the right figure which plotted the propagations of the same laser probes over a large range of 0~100m. In addition we see by close observation that at large distances the X-directional distance between a red (or green) line and an adjacent blue line approaches one forth of the X-directional distance between two adjacent blue lines. This phenomenon could be explained as follows.

From $Z=Z_0$ to $Z=Z_0+\Delta Z$, the X-directional distance between a red (or green) line and an adjacent blue line increases from zero to $\Delta d_{1,2}$ as described by Eq.4, meanwhile the X-directional distance between adjacent blue lines changes from ΔX to $\Delta X'$. It is easy to find that,

$$\frac{\Delta X}{Z_0} = \frac{\Delta X'}{Z_0 + \Delta Z} \qquad (13)$$

Rearrange Eq.13 as,

$$\Delta X' = \frac{\Delta X}{Z_0}(Z_0 + \Delta Z) \qquad (14)$$

Dived Eq.4 by Eq.14, we get,

$$\frac{\Delta d_{1,2}}{\Delta X'} = \frac{D}{2\Delta X} \frac{\Delta Z}{Z_0 + \Delta Z} \qquad (15)$$

From Eq.15 we can see that $\Delta d_{1,2}/\Delta X'$ approaches 1/4 when $\Delta Z >> Z_0$. It could also be seen that $\Delta d_{1,2}/\Delta X'$ becomes -1/4 when $\Delta Z = -Z_0/2$. In combination, start from $Z_0/2$ to infinity, both red and green lines are centred round blue lines with X-directional deviations no larger than one fourth of the X-directional distances between adjacent blue lines at the same distance, obtaining no chance to intersect with each other. It implies that no ambiguity would occur if the laser probes with preset destinations at Z_0 are used to measure the depth of an object located within the range from $Z_0/2$ to infinity. As shown in Fig.13a using laser probes with preset destinations at Z_0=2m, from monitored pictures we can definitely tell whether there is an object and where it is within the range of 1~100m if we search round the
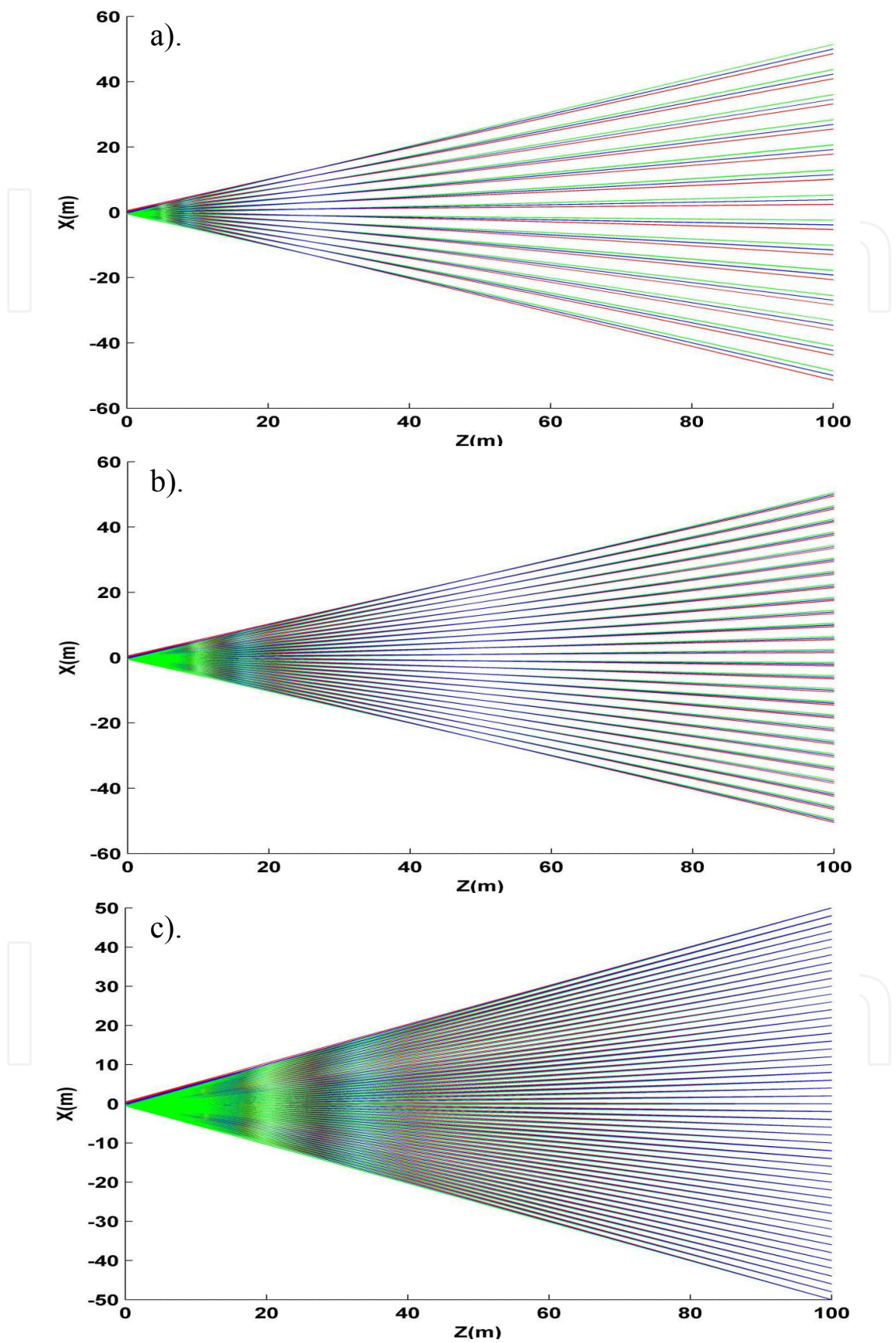
Fig. 14. Propagations of laser probes with destinations at a). 26m; b). 50m; and c). 100m.

preset image position A' and confine the searching pixel range Δj less than one fourth of the pixel number between two adjacent preset image positions. Since N_p preset points distribute evenly over a width of W, which cover a total of N pixels, $\Delta j \leq N/4N_p$. If N=1000, $\Delta j \leq 125$.

Next lets check Fig.13b for $Z_0=4m$. Using Eq.12, we have $N_p=3$. Since the maximum value for n in Eq.11 is $N_p-1=2$ and n should be even integer, we have n=0, 2. It means that beside 3 preset points there is $N_p-n=3-2=1$ extra cross point at $Z=Z_0/5=0.8m$, which are clearly seen in the left figure in Fig.13b. The number of extra cross points decreases by n because $j=(k+i)/2=k-n/2$ as required by Eq.10c is unable to adopt every number from 1 to N_p. As discussed above using laser probes with preset destinations at $Z_0=4m$, from captured pictures we can definitely tell whether there is an object and where it is within the range of 2~100m if we confine the searching pixel range to $\Delta j \leq N/4N_p$. If N=1000, $\Delta j \leq 83$.

Similarly both the preset points and the extra cross points are observed exactly as predicated by Eq.12 for $Z_0=8,14,26,50$, and 100m as illustrated in Fig.13c-d and Fig.14. With above arrangement a wide object at a certain distance Z might be hit by laser probes with preset destinations on different planes, while a narrow object might still be missed by all above laser probes since the X-directional spaces between adjacent laser probes are now more than $\Delta X=2m$ if $Z>Z_0$, although they decrease to $\Delta X/2=1m$ at $Z_0/2$. To detect narrow objects we may add another 100 gropes of laser probes with same preset destinations at Z_0 but on different planes perpendicular to Y-Z plane, each grope shifting $\Delta X/100=20mm$ along X-directional as illustrated in Fig.15. With all these laser probes a slender object as narrow as 20mm, see the object O_1 in Fig.15a, would be caught without exception at a single measurement. But if an object is not tall enough to cover several rows of laser probes, see the object O_2 in Fig.15a, it may also escape from detection. To increase the possibility of detecting objects with small height we may re-arrange the positions of the laser probes by inserting each row of laser probes from the lower half part into every row of laser probes at upper half part. As a result the maximum X-directional shift between adjacent rows of laser probes reduces from 2-0.02=1.98m to 1m as illustrated in Fig.15b. As could be seen the same object O_2 now gets caught by a laser probe in the fourth row.
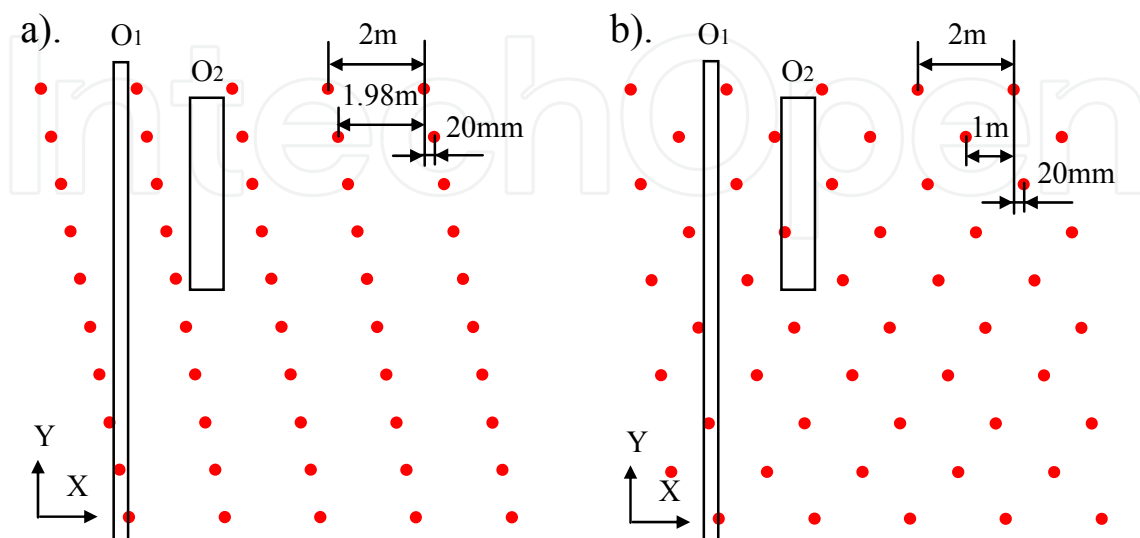

Fig. 15. Arrangements of laser probes with same destination on the X-Y plane.

In above design we arranged 100 group of laser probes with destinations at Z_0=2,4,8,14, 26,50, and 100m respectively. That is to say a total of $100\times(1+3+5+8+14+26+51)+1$=10801 laser probes have been employed. With so many laser probes an object as narrow as 20mm might be detected within a single measurement, or a single frame, without ambiguity. If the object is located between 50 and 100m, it could be detected correctly by any laser probe hitting on it. If it comes closer to the camera, although it might be incorrectly reported by laser probes with destinations at Z_0=100m, or 50m, etc, it will be correctly reported by laser probes with destinations at smaller Z_0. Considering the facts that the measuring range of the laser probes overlap greatly, the X-directional space between adjacent laser probes reduces by a half at $Z_0/2$ than that at Z_0, and the car bearing the camera, or the object itself, is moving, an object as narrow as 10mm or much less has great chance to be detected, or hit by at least one laser probe, within one or several frames.

3.3 Real-time large volume full field 3D measurement

Usually a laser probe 3D camera discussed in previous subsection could acquire at maximum about 10^4 three dimensional coordinates every frame using 8-bit SLMs. If dense three dimensional coordinates need to be acquired in real time a laser probe 3D camera could be incorporated with a pair of stereovision cameras. The accurate three dimensional coordinates come directly from the laser probe 3D camera plus those derived from stereovision make a complete description of the full field. More importantly, the laser probe 3D camera helps greatly in matching, noise depression and calibration for stereovision. As illustrated in Fig.16, a pair of digital cameras $C_{1,2}$ for stereovision have been added to the device in Fig.8, which are separated by a distance of D_1. D_1 might adopt a value larger or
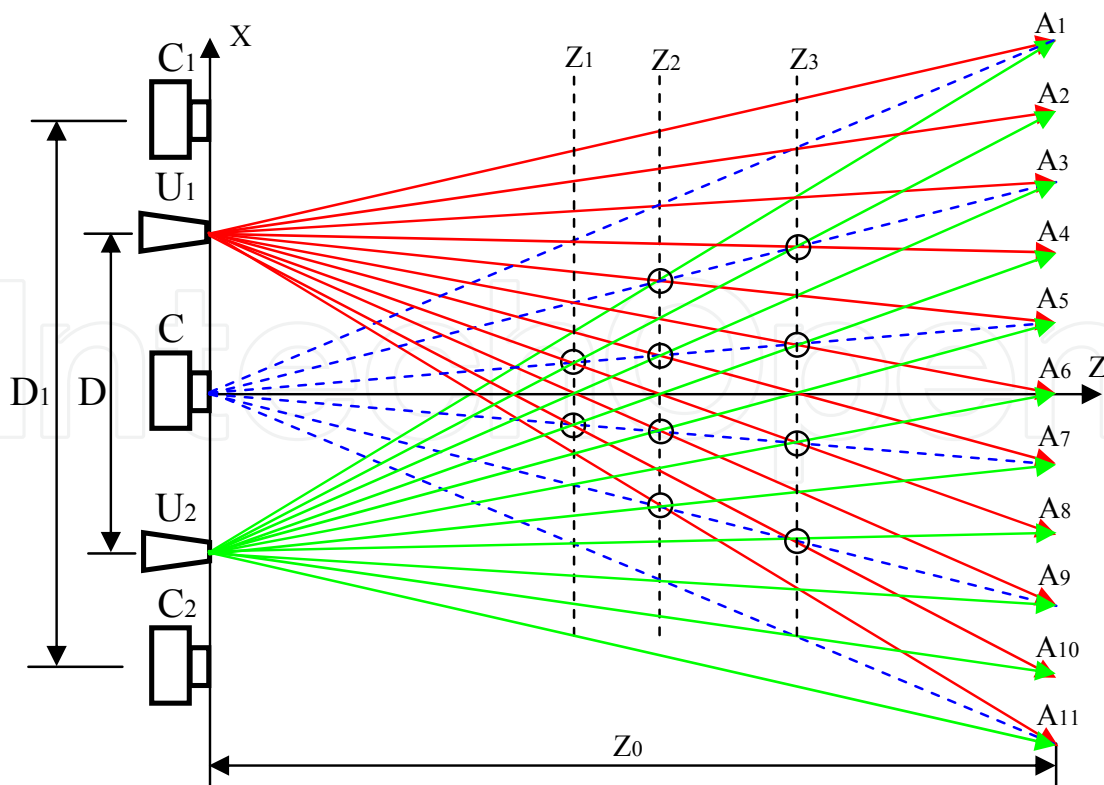

Fig. 16. A laser probe 3D camera combined with a stereo vision camera.

smaller than D. Each laser probe puts a mark on the object. From the image captured by camera C the absolute location of the object could be calculated using Eq.5 and the positions of the same mark on the pictures captured by camera C_1 and C_2 could then be predicated. In other word, one mark on the pictures captured by camera C_1 could easily be matched with the same mark on the pictures captured by camera C_2. Without these marks the matching between the pictures captured by cameras C_1 and C_2 might be very difficult or impossible over many pixels, creating serious noises in 3D reconstruction. The matching of the rest pixels around the marks could be performed quickly with reduced searching range. The marks also serve as an accurate and efficient means for the calibration of cameras C_1 and C_2. In stereovision it is very important to align one camera accurately with another camera, which brings great trouble when changing the focal length of one camera to zoom in or out, since the same amount of changes must be made instantly to the focal length of another camera. With the help of the laser marks, one camera needs only to follow roughly the changes of another camera. This is because all the pictures captured by cameras are projections of objects on the image plane, which is determined by the location, orientation and the focal length of the camera. Usually camera C is fixed at the origin of coordinates as illustrated in Fig.16. The only unknown parameter $tg\alpha$ in Eq.5, which is related to the focal length, is pre-calibrated. It could also be determined on the spot for every picture captured by camera C based on the fact that the same object detected by neighbouring laser probes with different preset destination Z_0 should have nearly the same depth Z as predicated by Eq.5. Even for very rough objects $tg\alpha$ could be properly determined after a least squares fit over the depths of many pairs of neighbouring laser probes. Next the unknown locations, orientations and the focal lengths of the camera $C_{1,2}$ could be derived from the image positions of hundreds of laser probes whose absolute coordinates are pre-calculated using Eq.5. Then by stretching, or rotation, or a combination of them, the pictures come from camera C_1 could easily be transformed to match with the pictures from camera C_2. After above pre-processing, stereo matching might be performed on the overlapped region of the image pairs from camera $C_{1,2}$.

When laser probes are arranged as discussed in previous subsection, we say that the laser probe 3D camera is working in detection mode. For continuous measurements, once the location of all the objects are found in a frame, laser probes could be rearranged much more densely near the surfaces of known objects so that more three dimensional coordinates could be acquire within successive frames. In this case we say that the laser probe 3D camera is working in tracing mode. After some frames in tracing mode, a laser probe 3D camera should return to detection mode for one frame to check whether there are new objects appearing in the field. In Fig.16 the number of laser probes increased to 11 for tracing mode. It could be seen that as the number of laser probes increases the number of extra crossing points also increases as compared with that in Fig.11. Nevertheless these extra cross points are harmless since we already known the object lies around Z_0, away from Z_1 to Z_3.

The stereovision pictures recorded by cameras $C_{1,2}$ bear the images of lots of laser probes. They are harmful for later 3D display. Although these marks could be cleaned away via post imaging processing, a more preferable approach is to separate the visible light from infrared laser probes with a beam splitter. As illustrated in Fig.17, the beam splitter BS reflects the infrared laser probes onto image transducer CCD_1, while passing the visible light onto image transducer CCD_2. The advantage to employ two image transducers within one camera

is that the electronic amplifier for each image transducer may adopt a different gain value so that the dark one does not get lost in the bright one. This is beneficial especially when working in strong day light. If both cameras C_1 and C adopted the same structure as illustrated in Fig.17, camera C_2 could be taken away because images for visible light from cameras C_1 and C are enough to make up a stereovision.
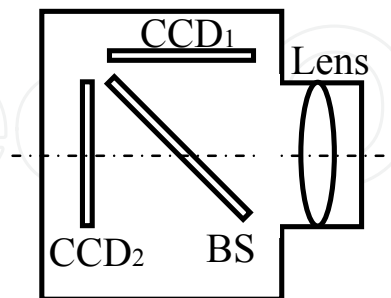

Fig. 17. A digital camera capable of recording infrared and visible light images separately.

3.4 Static large size or 360-deg shape measurement

In shape measurement for industry inspection the measuring accuracy is more crucial than measuring speed. Usually the component under investigation stays at a fixed position or moves slowly on a line during measurement. To improve measuring precision we can first divide the entire area under investigation into lot of subdivisions, say 10×10 subdivisions. Then measure each subdivision with much improved depth resolution due to reduced view angle as discussed in section 2. Dense and accurate three dimensional coordinates of the entire area could be obtained by patching all the measurements together [Gruen, 1988; Heipke, 1992]. The patching or aligning between adjacent subdivisions becomes easy and accurate with the help of laser probes. We can arrange adjacent subdivisions in a way so that they overlap slightly. As illustrated in Fig.18, when shifting from one subdivision S_1 to an adjacent subdivision S_2 we move the camera C and laser probe generating units $U_{1,2}$ separately. First we move the camera C to the new subdivision S_2 and keep $U_{1,2}$ unchanged, see Fig.18b. From the images of laser probes on the overlap region on the pictures taken before and after the movement of camera C, we can find exactly how much the camera C have moved. This could be accomplished using the fact that the laser probes on the overlap region stay at fixed positions. Next we move $U_{1,2}$ to the new subdivision S_2 with the camera
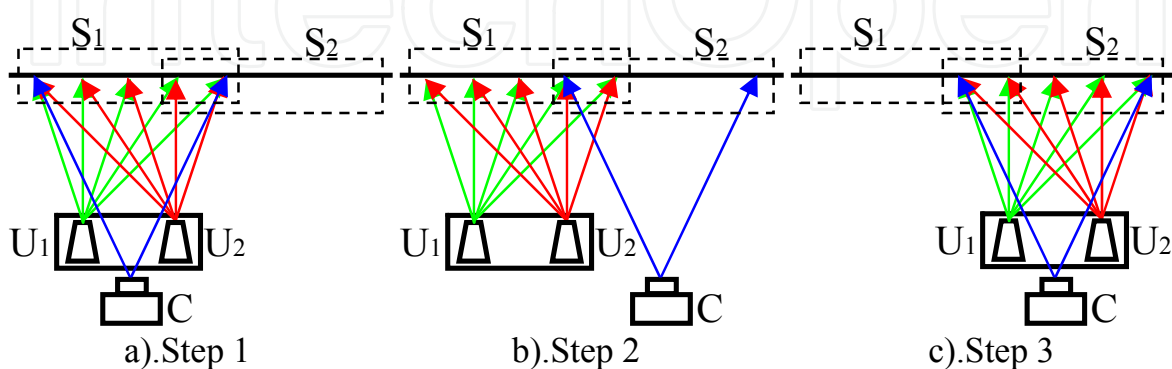

Fig. 18. Steps to move laser probe generating unit $U_{1,2}$ and camera C separately to adjacent subdivision.

C unchanged, see Fig.18c. From captured picture before and after the movement of $U_{1,2}$ the exact displacement could be calculated from the displacements of the same laser probes. Then measurement on the new subdivision S_2 could be carried out.

For 360-deg shape measurement, we can mount the two laser probe generating units $U_{1,2}$ and the camera C on two separate circular tracks, with the object under investigation placed at the centre. When the measurement at a certain angle is done, the camera C and laser probe generating units $U_{1,2}$ could be move to a new view angle separately following the same strategies as discussed above. With the help of laser probes on the overlapped region we can determine over how much angle have $U_{1,2}$ and camera C each moved, which makes it easy to transfer the local coordinates at a certain view angle accurately to the global coordinates. Otherwise additional measure has to be taken to monitor the positions of $U_{1,2}$ and camera C.

In shape measurement we can chose CCD or CMOS image sensors with large pixel number to achieve high vertical and lateral resolution at the cost of reduced frame rate. Usually shape measurements are carried out at small fixed distances, if we let D = 2Z, Eq.6 simplifies to,

$$dZ = \frac{W}{N} dj_{1,2} \qquad (16)$$

Eq.16 implies that the vertical resolution is the same as the lateral resolution determined by the image sensor. When an image sensor with a total of 10k×10k pixels is used, we have N=10000. Then for a subdivision with an area of 100×100mm^2, i.e., W=100mm, both vertical and lateral resolutions reach 5μm for $dj_{1,2}$=0.5. By a least squares fit method sub-pixel resolution for the image position of laser probes are possible [Maalen-Johansen, 1993; Clarke, et al., 1993]. When 1/20 sub-pixel resolution is obtained after least squares fit, $dj_{1,2}$=0.05, above said resolution improves to 0.5 μm and the relative error reaches 5×10^{-6}.

As discussed in subsection 3.2 within a single frame about 10801 points could be acquired using a laser probe 3D camera, each providing a three dimensional coordinate for the detected object. Usually this number of three dimensional coordinates is enough for industry inspection. The feature sizes, such as width, height, diameter, thickness, etc., could all be derived from measured data. If dense coordinates are needed for very complex shapes, they could be acquired from successive frames. For example, within 100 successive frames, which last 10 seconds at a frame rate of 10f/s, a total of about 100×10801≈10^6 three dimensional coordinates could be acquired. Between each frame the laser probes shift a little their preset positions along horizontal or vertical direction. When combined together these 10^6 three dimensional coordinates provide a well description of the entire component. In addition, to detect possible vibrations of the object during successive frames we can fix the positions of a small fraction of laser probes throughout the measurements. The movements of the images of these fixed laser probes help to reveal and eliminate the movements of the objects relative to the camera.

4. Characteristics of laser-probe 3D cameras

In previous section we discussed four typical configurations of laser probe 3D cameras and their measuring precision. In this section we will provide more analysis concerning such

characteristics as processing speed, power consumption, and resistance to external interferences and compare them with that of other measuring methods.

4.1 Image processing speed

The processing, or the derivation of depth information from pictures captured by a laser probe 3D camera is simple compared with many other methods like structured light projection, stereovision, etc. One need only to search on the left and right side of pre-known image positions of preset laser probes to see whether there is a pair of light spots reflected by objects. In other words one need only to check whether there are local intensity maximums, or whether the image intensities exceed a certain value on the left and right sides of N_p pre-known pixels with a searching range of $\pm N/4N_p$ pixels. The searching stops once the pair of light spots is found. Therefore on one image row, a total of $N_p \times 2N/4N_p$ $=N/2$ pixels need to be checked at maximum. Considering pairs of light spots reflected by objects lie symmetrically around pre-known image positions, when one light spot is detected another light spot could be found easily on other side after one or two steps of searching. It implies that the maximum searching steps could be reduced to about $N/4$. Usually the pre-known pixels are arranged on every other row, so only about one eighth of the total pixels of an image need to be checked. Once a pair of light spots is detected the depth of the object could be calculated easily using Eq.5 with less than 10 operations. For the laser probe 3D camera given in the last section, at most 10801 points need to be calculated. Since the working frequencies of many ARM, FPGA chips have reached 500MHz~1 GHz, one operation could be perform within 100ns on many embedded systems. Then the total time to calculate 10801 points is less than $10801 \times 10 \times 100ns \approx 0.01s$. It means that an obstacle in front of a car could be reported within a single frame.

4.2 Laser power

Since the laser power is focused into each laser probe rather than projected over the entire field, a laser probe 3D camera may be equipped with a relatively low power laser source. For micro 3D measurement a laser power less than 20mW might be enough, because almost all the laser energy might be gathered by objective lens and shed onto the image transducer except the adsorption by SLMs and optical lenses. However if optical manipulation of micro- or nano-particles is to be carried out higher energy might be necessary [MacDonald, 2002; Grier, 2003]. For industry inspection a laser power less than 2W might be enough since the measurements are usually carried out within about 1m. For obstacle detection within a range of 1~100m, if on average 1~5mW should be assigned to each laser probe for a total of 10801 laser probes, considering an adsorption of 90% by SLMs and optical lenses, a laser power of 100~500W might be necessary. To reduce energy adsorption dedicated gray scale SLMs should be employed. In a gray scale SLM the colour filters could be omitted, which results in triple decrease of energy adsorption as well as triple increase of available pixel number. In addition, among said 10801 laser probes, those with preset destinations at near distances might be assigned with much lower energy. Therefore the total energy for a laser probe 3D camera to measure an area of 100m×100m at a distance of 100m might be reduced to within 20~100W, much less than the lamp power in a LCD projector. The laser power could be further reduced by several times if sensitive CCD or CMOS image sensors are

employed. Other optical methods could hardly work with such low light power over so large area. For example, in structured light projection method, if an output light energy of 20~100W is projected over the same area, the illuminating intensity is only 2~10mW per square meter. In contrast, at a distance of 100m, the diameter of a laser probe could be as small as ~10mm as discussed in section 2. It means that even with an average energy of 1~5mW, the illuminating intensity provide by each laser probe could reach $1\sim5mW/25\pi$ per square millimetre, which is about 15708 times higher than that available in structured light projection method at the same distance.

4.3 Resistance to interferences

There are various interferences that may decrease measuring accuracy, to name a few, environmental light, vibration, colour, reflectivity and orientation of the object under investigation, etc. In subsection 3.3 we discussed how to eliminate the influence of environment light with a beam splitter. In subsection 3.4 we introduced a method to detect and eliminate the vibration of an object during successive measuring frames. Since a laser probe 3D camera determines the absolute location of an object by the positions rather than the exact intensities of reflected images of laser probes that are focused with diffraction limited precision, the colour, reflectivity or orientation of the object exerts limited influence on the measuring results, especially in fast obstacle detection.

There is another interference source that usually receives little attention but is of vital importance in practice, i.e., mutual interferences between same active devices. When several users turn on their laser probe 3D cameras at the same time, will every camera produce good results like it usually does when it works alone? It is true that one camera would now capture the laser probes projected by other cameras. Fortunately few of the images of laser probes projected by other cameras would lie symmetrically round the pre-known image positions of the laser probes projected by itself, since the laser probes from different devices are projected from different places with different angles. In image processing, to depress this mutual interference, we can discard all the single light spots or pairs of light spots lying asymmetrically round the pre-known image positions. In addition, referring Fig.15, we may store in each camera many sets of laser probe arrangements that differ in their vertical pattern, or rotated with a different angle within the vertical plane. When it observed the existence of laser probes from other cameras by turning off its own laser probes, it may chose one arrangement of laser probes that coincides least with existing laser probes. Considering the number of laser probes projected by one camera is about 100 times less than the camera's total pixel number, about ten cameras might work side by side at the same time without much interference to each other. In addition a laser probe 3D camera could also distinguish its own laser probes from that emitted by other cameras from at least 4 successive frames with its own laser probes turning on and off repeatedly. Those light spots that appear and disappear properly are very likely the images produced by its own laser probes. Further more, for a professional laser probe 3D camera, several laser sources with different wavelengths may be incorporated. Accordingly narrow band changeable beam splitters should be used in Fig.17. When other cameras exist, it may shift to a least occupied wavelength. With all above strategies several tens of laser probe 3D cameras may work well side by side at the same time.

5. Conclusion

In summary, the chapter puts forth a laser probe 3D camera that offers depth information lost in conventional 2D cameras. Via digital optical phase conjugation, it projects hundreds and thousands of laser probes precisely onto preset destinations to realize accurate and quick three dimensional coordinate measurement. A laser probe 3D camera could be designed with vertical and lateral resolutions from sub-micrometer to several micrometers for micro object or medium sized component measurement. It could also be configured for real-time 3D measurement over a large volume—for example, over a distance of 1~100m with a view angle larger than 50°—and detect any obstacle as narrow as 20mm or much less within a single frame or 0.01 second, which is of great use for auto-navigation, safe-driving, intelligent robot, etc.

The laser probes in a 3D camera not only make a 3D measurement simple and quick, but also help a lot in accurate patching for large size or 360-deg shape measurement, monitoring and elimination of vibration, depression of mutual influence when many laser probe 3D cameras work side by side, etc. When incorporated with stereovision they make the stereo matching easy and accurate. More than that, they offer an efficient means for camera calibration so that when one camera zooms in or out, another camera may follow only roughly rather than exactly, alleviating the stringent equipment requirements in stereo movie industry.

With its diffraction limited resolution to digitally reconstruct any optical wavefront, however complex it is, digital optical phase conjugation opened a way for many new techniques. The laser probe 3D camera discussed in the chapter is only one of the many possible applications. Since huge number of laser probes with varying intensity could be created precisely at lots of preset points, pointing more laser probes into each preset point using a large array of laser probe generating units and taking one such preset point as a 3D pixel, real-time true 3D display over a very large space with fine quality could become a reality. High power laser beams could also be formed, accurately focused and steered via digital optical phase conjugation, which may find wide applications in such fields as nuclear fusion, space laser communication, and so on. In micro world arrays of laser probes with sub-micrometer resolution could be employed for fast micro- or nano-partical assembling, operations on DNA, stereo information storage, etc.

6. Acknowledgment

7. References

Amako, J.; Miura, H. & Sonehara, T. (1993). Wavefront control using liquid-crystal devices, *Appl.Opt.*, Vol.32, No.23, pp.4323-4329.

Asim, B. (2008). *Stereo Vision*, InTech, ISBN: 978-953-7619-22-0, Vienna, Austria.

Barbosa, E. A. & Lino, A. (2007). Multiwavelength electronic speckle pattern interferometry for surface shape measurement, *Appl. Opt.*, Vol.46, pp.2624–2631.

Chen, F.; Brown, G. M. & Song, M. (2000). Overview of three-dimensional shape measurement using optical methods, *Opt. Eng.* Vol.39, No.1, pp.10–22.

Clarke, T.A.; Cooper, M.A.R. & Fryer, J.G.(1993). An estimation for the random error in sub-pixel target location and its use in the bundle adjustment, *Proc.SPIE*, Vol.2252, pp.161-168.

Feinberg, J. (1982). Self-pumped continuous-wave phase-conjugation using internal reflection, *Opt.Lett.,* Vol.7, pp.486.

Grier, D.G. (2003). A revolution in optical manipulation, *Nature,* Vol.424, pp.810-816.

Gruen, A.W. (1988). Geometrically constrained multiphoto matching, Photogramm. *Eng. Remote Sens.,* Vol.54, No.5, pp.633-641.

Guan, C.; Hassebrook, L.G. & Lau D.L. (2003). Composite structured light pattern for three-dimensional video. *Opt Express,* Vol.11, pp.406–417.

Heipke, C. (1992). A global approach for least squares image matching and surface recognition in object space, *Photogramm. Eng. Remote Sens.,* Vol.58, No.3, pp.317-323.

Leonhardt, K; Droste, U. & Tiziani, H.J. (1994). Microshape and rough surface analysis by fringe projection, *Appl. Opt.,* Vol.33, pp.7477-7488.

Jürgen, K. & Christoph S. (2011), Address-event based stereo vision with bio-inspired silicon retina imagers, In: *Advances in theory and applications of stereo vision,* Asim Bhatti, pp.165-188, InTech, ISBN:978-953-307-516-7, Vienna, Austria

Kohler, C.; Schwab, X. & Osten, W. (2006). Optimally tuned spatial light modulators for digital holography, *Appl.Opt.,* Vol.45, No.5, pp.960-967.

Maalen-Johansen, I.(1993). On the precision of sub-pixel measurements in videometry, *Proc.SPIE,* Vol.2252, pp.169-178.

MacDonald, M.P., et al. (2002). Creation and manipulation of three-dimensional optically trapped structures, *Since,* Vol.296, pp.1101-1103.

Matoba, O., et al. (2002). Real-time three-dimensional object reconstruction by use of a phase-encoded digital hologram, *Appl.Opt.,* Vol.41, No.29, pp.6187-6192.

Moring, I. (1989). Active 3-D vision system for automatic model-based shape inspection, *Opt. Lasers Eng.,* Vol.10, pp.3-4.

Neto, L.G.; Robergy, D.; & Sheng, Y. (1996). Full-range, continuous, complex modulation by the use of two coupled liquid-crystal televisions, *Appl.Opt.,* Vol.23, No.23, pp.4567-4576.

Srinivasan, V.; Liu, H.C. & Halioua M. (1984). Automated phase-measuring profilometry of 3-D diffuse objects. *Appl Opt.,* Vol.23, pp.3105–3108.

Stephan, H.; Thorsten, R & Bianca, H. (2008). A Performance Review of 3D TOF Vision Systems in Comparison to Stereo Vision Systems, In: *Stereo Vision,* Asim Bhatti, pp.103-120, InTech, ISBN: 978-953-7619-22-0, Vienna, Austria.

Tudela, R., et al. (2004). Wavefront reconstruction by adding modulation capabilities of two liquid crystal devices, *Opt.Eng.,* Vol.43, No.11, pp.2650-2657.

Yamaguchi, I. et al. (2006). Surface shape measurement by phase-shifting digital holography with a wavelength shift, *Appl. Opt.,* Vol.45, pp.7610–7616.

Yariv, A. & Peper, D.M. (1977). Amplified reflection, phase conjugation, and oscillation in general four wave mixing, *Opt.Lett.,*Vol.1,No.1, p.16.

Zhiyang, L. (2010a). Accurate optical wavefront reconstruction based on reciprocity of an optical path using low resolution spatial light modulators, *Optics Communications,* Vol. 283, pp.3646-3657. (2010b). *SciTopics.* Retrieved December 30, 2010, from http://www.scitopics.com/Real_time_accurate_optical_wave_front_reconstruction_based_on_digital_ optical_phase_conjugation.html

Digital Image Processing

Edited by Dr. Stefan G. Stanciu

This book presents several recent advances that are related or fall under the umbrella of 'digital image processing', with the purpose of providing an insight into the possibilities offered by digital image processing algorithms in various fields. The presented mathematical algorithms are accompanied by graphical representations and illustrative examples for an enhanced readability. The chapters are written in a manner that allows even a reader with basic experience and knowledge in the digital image processing field to properly understand the presented algorithms. Concurrently, the structure of the information in this book is such that fellow scientists will be able to use it to push the development of the presented subjects even further.

INTECH

open science | open minds